Scientific
Research

Analytic Approximations of Projectile Motion with Quadratic Air Resistance

R. D. H. Warburton[1], J. Wang[2], J. Burgdörfer[3]

[1]Department of Administrative Sciences, Metropolitan College, Boston University, Boston, USA; [2]Department of Physics, University of Massachusetts Dartmouth, North Dartmouth, USA; [3]Institute for Theoretical Physics, Vienna University of Technology, Vienna, Austria.
Email: rwarb@bu.edu

ABSTRACT

We study projectile motion with air resistance quadratic in speed. We consider three regimes of approximation: low-angle trajectory where the horizontal velocity, u, is assumed to be much larger than the vertical velocity w; high-angle trajectory where $w \gg u$; and split-angle trajectory where $w \sim u$. Closed form solutions for the range in the first regime are obtained in terms of the Lambert W function. The approximation is simple and accurate for low angle ballistics problems when compared to measured data. In addition, we find a surprising behavior that the range in this approximation is symmetric about $\pi/4$, although the trajectories are asymmetric. We also give simple and practical formulas for accurate evaluations of the Lambert W function.

1. Introduction

In a previous paper on projectile motion with air resistance linear in speed, we presented closed form solutions for the range in terms of the Lambert *W* function [1]. Amid the growing list of problems that benefited from using the *W* function [2–7], one question naturally arises as to whether a similar approach exists if air resistance is quadratic in speed, the more realistic case in practice.

We have studied this problem and found that solutions exist for low-angle trajectories using the *W* function. In this paper, we report our findings, starting with an overview of the regimes of approximation in Section 2. We focus on the low-angle regime in Section 3 and discuss the dynamics, which leads to a remarkable property that the range is symmetric about $\pi/4$, even in the presence of air resistance. For completeness, high-angle and split-angle regimes are briefly discussed in Section 4 and 5, respectively, followed by a comparison with observed data and discussions in Section 6. To make the *W* function easily accessible, in the Appendix we give simple and practical formulas for the accurate evaluation of this function.

2. Regimes of Approximation

We assume the net force $\vec{F}$, including air resistance and

gravity on the projectile of mass, m, to be $\vec{F} = -mbv\vec{v} -mg\vec{j}$. This leads to the equations of motion as

$$\frac{du}{dt} = -bvu, \quad \frac{dw}{dt} = -buw - g, \qquad (1)$$

where *b* is the drag coefficient with the dimensions m^{-1}. The components of the velocity are $\vec{v} = u\vec{i} + w\vec{j}$, with $u = dx/dt$ and $w = dy/dt$, where *x* and *y* are the usual horizontal and vertical positions of the projectile. The initial position of the projectile is at the origin. Throughout the paper, we use the following notations for frequently occurring terms:

u_0, w_0 = initial horizontal and vertical velocities;

$R_0 = \dfrac{2u_0 w_0}{g}$ = range with no air resistance;

$$\beta = b\frac{2u_0 w_0}{g} \equiv bR_0 \qquad (2)$$

To our knowledge, closed form solutions to (1) are known only for special initial conditions, not for arbitrary initial conditions [8]. The difficulty is with the coupling of *u* and *w* in the speed $v = \sqrt{u^2 + w^2}$ which makes the problem inseparable. Further approximations are necessary to solve (1) analytically.

We consider three approximations aimed at linearizing the speed according to the relative magnitudes of u and w: low-angle trajectory (LAT) approximation, $u \gg w$; high-angle trajectory (HAT) approximation, $w \gg u$; and split-angle trajectory (SAT) approximation, $u \sim |w|$, as,

$$v = \sqrt{u^2 + w^2} \approx \begin{cases} u & if \ u \gg w, LAT \\ |w| & if \ |w| \gg u, HAT \\ \sqrt{2}u \ (or \ |w|) & if \ u \gg |w|, SAT \end{cases} \quad (3)$$

Each of the approximations will be discussed below, with the emphasis on LAT that is important in practice and in ballistics.

3. Low-Angle Trajectory (LAT) Approximation

3.1 The Trajectory

We assume in this case the horizontal velocity is on average much greater than the vertical velocity, $u \gg w$. This will be the case if the firing angle is small, a case also discussed by Parker [9]. Here the speed may be approximated as $v \approx u$ according to (3), so that the equations of motion in the LAT approximation are

$$\frac{du}{dt} = -bu^2, \quad \frac{dw}{dt} = -buw - g. \quad (4)$$

One can solve for u first, after which w, x, and y can be obtained. Hereafter, we will omit non-essential intermediate steps. The solutions may be verified by substitution into the equations of motion. The solutions are

$$u = \frac{u_0}{1 + at}, \quad w = \frac{w_0 - gt/2}{1 + at} - \frac{1}{2}gt, \quad a \equiv bu_0, \quad (5)$$

$$x = \frac{1}{b}\ln(1 + at), \quad y = \left(w_0 + \frac{g}{2a}\right)\frac{1}{a}\ln(1 + at) - \frac{1}{4}gt^2 - \frac{gt}{2a}. \quad (6)$$

Equation 6 gives the trajectory in the LAT approximation.

The trajectories computed from (6) are plotted in **Figure 1** for three angles: 20°, 45°, and 70°. The initial speed is 9.8 m/s for all angles. The drag coefficient is $b = 0.1m^{-1}$.

For comparison, we also show the trajectory from ideal projectile motion with no air resistance and the trajectory from the solutions with the full v^2 air resistance, Equation 1. We will simply refer to the former as the ideal motion, and the latter as the full solution.

The full solution is carried out by numerically integrating the equations of motion with the full v^2 resistance (1), using the Runge-Kutta method. (The two curves labeled HAT and SAT in **Figure 1** are discussed in Sections 4 and 5.)

The agreement between the LAT approximation and

the full solution is good at 20° (nearly indistinguishable in **Figure 1(a)**), and it becomes worse for larger angles. This is as expected since the assumption was that LAT is valid only at small angles. The range is much reduced compared to the ideal motion. Air resistance introduces in the trajectories a well-known backward-forward asymmetry. The ascending part of the trajectory is shallower and longer, and the descending part is steeper and shorter.
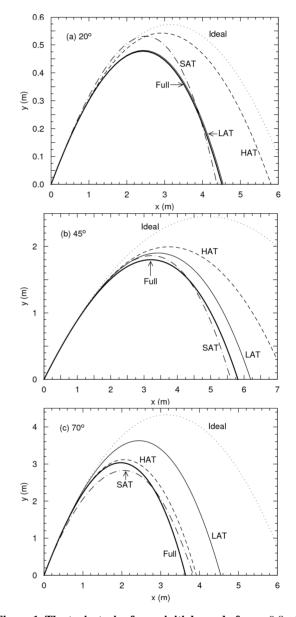

Figure 1. The trajectories for an initial speed of $v_0 = 9.8$m/s and drag coefficient $b = 0.1$m^{-1} at three firing angles, 20° (a), 45° (b), and 70° (c). The labeled curves are (see text): Full (thick solid line) - the numerical solution with the full v^2 resistance; LAT (solid line); HAT (dashed line, see Section 4); SAT (dash-dotted line, see Section 5), Ideal (dotted line) - motion without air resistance

3.2 The Range and Height in Comparison with Measurements

To find the range of the projectile we eliminate t from (6) to obtain

$$y = \left(w_0 + \frac{g}{2a} \right) \frac{x}{u_0} - \frac{g}{4a^2} \left(\exp(2bx) - 1 \right). \qquad (7)$$

The range, R, is the value of x when $y = 0$. It satisfies

$$\left(w_0 + \frac{g}{2a} \right) \frac{R}{u_0} - \frac{g}{4a^2} \left(\exp(2bR) - 1 \right) = 0. \qquad (8)$$

This is a transcendental equation that until now had been customarily solved numerically or graphically [9]. But as we reported [1], equations of this type can also be solved analytically, with the results written in closed form in terms of the Lambert W function.

The Lambert W function [10] is defined, for a given value z, as the (inverse) function satisfying

$$W(z) \exp(W(z)) = z. \qquad (9)$$

Our discussions below refer closely to the properties of this relatively "new" function. For readers unfamiliar with this function, we give a brief review in the Appendix. There the reader will also find some practical formulas for evaluating W.

To solve for the range R in terms of W, (8) needs to be rearranged in the form of (9) such that the multiplicative prefactor to the exponential, $W(z)$, is the same as the exponent. This can be achieved by following the steps in [1]. The result is

$$\left[-2bR - \frac{1}{1+\beta} \right] \exp \left[-2bR - \frac{1}{1+\beta} \right] = -\frac{1}{1+\beta} \exp \left[-\frac{1}{1+\beta} \right], \qquad (10)$$

with defined in (2). We identify from (9) and (10) that

$$W(z) \equiv \left[-2bR - \frac{1}{1+\beta} \right], \text{ or } R = -\frac{1}{2b} \left[W(z) + \frac{1}{1+\beta} \right],$$

$$z = -\frac{1}{1+\beta} \exp \left[-\frac{1}{1+\beta} \right] \qquad (11)$$

This is the closed form expression for the range, R, in the LAT approximation.

The height, H, can be obtained by maximizing y in (7), and is given by

$$H = \frac{w_0}{2bu_0} \left[\frac{1+\beta}{\beta} \ln(1+\beta) - 1 \right]. \qquad (12)$$

We compare in **Table 1** measured range and height data with calculations from Equations 11 and 12 for firing angles less than one degree. (The details of the calculations are given in the next subsection.)

Table 1 shows that the measured data [11] and the calculations agree well once the firing angle is above about 10 minutes of arc. The discrepancy between measurement and theory is due to the uncertainty in the value b (see **Table 1** caption), and not the approximation itself. Because the largest angle is still less than 1, higher order corrections are negligible. The relative error for the height is usually much larger than the relative error for the range. This is probably due to the difficulty in accurately measuring the relatively small height in this case.

The large errors in height and in range at the two smallest angles need not cause concern. It is due to the combination of exceeding difficulty in determining the small angle and the small height at the same time. Note that the diameter of the projectile and the height are of the same order of magnitude here. Overall, this example shows that if a reasonable b can be obtained, the LAT approximation should work well for low angle ballistics problems.

3.3 Analytic Properties of the Range

3.3.1 The Symmetry of Range in Firing Angle

The analytic Formula 11 enables us to immediately draw several surprising conclusions on the general properties of the range, R. Since z is a function of β which depends on the product $u_0 w_0 \propto \sin(2\theta_0)$ (θ_0 is the firing angle), we conclude that i) the range R is symmetric about $\pi/4$, that is to say, two firing angles θ_1 and θ_2 will lead to the same range if $\theta_1 + \theta_1 = \pi/2$ (see the LAT curves in

Table 1. Measured and calculated results for a projectile of mass m = 9.7 g, diameter d = 0.76 cm, and muzzle velocity 823 m/s. The measured data are taken from [11]. Results are calculated from the LAT approximation (11,12). The drag coefficient b = 1.05×10^{-3} m^{-1} is determined from $b = C\rho d^2/m$, where C = 0.15 is the recommended value [11], and ρ = 1.2 kg/m^3 is the air density

Firing Angle (min)		2	5	8	12	16	20	26	33	40	49
	Measured	91	183	274	366	457	549	640	732	823	914
Range, R (m)	Calculated	76	177	265	367	456	534	636	738	826	923
	Error, %	16	3.3	3.3	0.27	0.22	2.7	0.63	0.82	0.36	0.98
	Measured	0.02	0.1	0.19	0.33	0.61	1.0	1.5	2.3	3.2	4.5
Height (m)	Calculated	0.011	0.068	0.17	0.36	0.62	0.93	1.5	2.3	3.2	4.5
	Error, %	45	32	11	9.1	1.6	7.0	0.0	9.5	3.2	2.2

Figures 1(a) and (c)); and ii) because $W(z)$ is a monotonic function, the maximum range occurs at $\pi/4$ [12]. Remarkably, these properties i) and ii) with air resistance in the LAT approximation are exactly the same as for ideal projectile motion *without* air resistance.

Given initial conditions u_0 and w_0, the range, R, can be computed from (11). Since z is negative and $W(z)$ is multi-valued (see Appendix) for $z < 0$, we have a choice of the branches W_0 or W_{-1}. Comparing z in (11) and (9) we identify one trivial solution, namely the primary branch,

$$W_0(z) = -\frac{1}{1+\beta} \qquad (13)$$

This solution, although mathematically correct, is unphysical because it gives a zero range when substituted into (11). The physical choice must be W_{-1}. We note that for linear resistance [1] the choices were the opposite, where W_0 was the physical solution and W_{-1} the unphysical one.

The range, R, calculated from (11) using W_{-1} is shown in **Figure 2** as a function of the firing angle. It clearly demonstrates that R is symmetric about, and maximum at, $\pi/4$. Also shown in **Figure 2**, for comparison, are the ranges for ideal projectile motion with no air resistance and with the full v^2 resistance.

Unlike the LAT case, the range of the full solution in **Figure 2** is not symmetric about $\pi/4$. It reaches maximum at an angle below $\pi/4$, a fact that is well known.
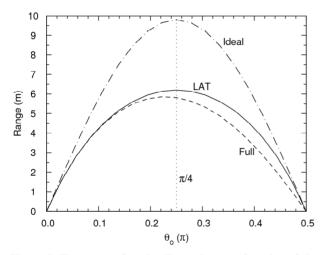

Figure 2. The range of projectile motion as a function of the firing angle θ_0. The initial speed is v^0 = 9.8 m/s and the drag coefficient is b = 0.1 m^{-1}. The LAT approximation (solid line) is maximum at and symmetric about $\pi/4$, as is the ideal motion (dash-dotted line). The range with the full v^2 resistance (dashed line) peaks before $\pi/4$, and is asymmetric

The LAT range is in good agreement with the full solution for low firing angles as expected, up to around $\pi/6$. Compared to the ideal case, the maximum ranges in the LAT and the full solutions are substantially reduced, by about 40% for this particular set of parameters.

We note that the LAT approximation produces asymmetric trajectories (**Figure 1**) but symmetric ranges. The physical reason can be traced to two factors influencing the range: the time of flight and the average horizontal velocity, as discussed below.

3.3.2 The Time of Flight and the Average Velocity

The average horizontal velocity, $\langle u \rangle$, and the time of flight, T, are related by

$$R = \langle u \rangle T. \qquad (14)$$

The time of flight T can be obtained from (6) by setting $x = R$, at $t = T$. Together with (11), this gives

$$T = \frac{\exp(bR)-1}{bu_0} = \frac{1}{bu_0}\left\{\exp\left[-\frac{1}{2}\left(W(z)+\frac{1}{1+\beta}\right)\right]-1\right\}. \qquad (15)$$

The average horizontal velocity can be expressed from (14) and (15) as

$$\langle u \rangle = \frac{u_0}{2}\left[W(z)+\frac{1}{1+\beta}\right]\left\{1-\exp\left[-\frac{1}{2}\left(W(z)+\frac{1}{1+\beta}\right)\right]-1\right\}^{-1}. \qquad (16)$$

Quantitatively, as the firing angle increases, the time of flight T increases, but the average horizontal velocity $\langle u \rangle$ decreases. However, before $\pi/4$, the increase in T is more than the decrease in $\langle u \rangle$ so that the range as governed by (14), increases. After $\pi/4$, however, the opposite happens so that the range decreases. The symmetric range is a result of the balance between T and $\langle u \rangle$.

3.3.3 The Range for Small and Large Air Resistance

In the limit of small air resistance, $b \to 0$, the dimensionless parameter β will be small, $\beta \to 0$. The argument z to the W in (11) approaches $z \to -1/e$, and $W(z) \to -1$ (see Appendix). Using the properties of $W(z)$ and after some algebra (we leave the details as an exercise to the interested reader), the first order correction to the range, R, in (9) is

$$R = R_0\left(1-\frac{2}{3}\beta\right) = R_0\left(1-\frac{2}{3}bR_0\right), \quad b \to 0, \qquad (17)$$

where R_0 is the range of ideal projectile motion, $b = 0$.

For large air resistance, $b \gg 1$ and $\beta \gg 1$. As $\beta \to \infty$, $z \to -1/\beta$ according to (11). Using the as-

ymptotic expressions for $W_{-1}(z \to 0) \approx \ln(z/\ln|z|)$ (see Appendix), we have from (11)

$$R = \frac{R_0}{2} \frac{\ln(\beta \ln \beta)}{\beta} \quad \text{with} \quad b, \beta \gg 1. \quad (18)$$

It is interesting to compare the scaling behavior with our earlier study [1] for linear resistance, where we found the range to scale as $1/b$, the inverse of the resistance. For quadratic resistance, (18) indicates $R \propto \ln(b \ln b)/b$. This shows that the logarithm term is characteristic of the quadratic resistance.

4. High-Angle Trajectory (HAT) Approximation

When the firing angle is large (close to $\pi/2$), we expect that, on average, the vertical velocity w will be much larger than the horizontal velocity, $|w| \gg u$. The speed is approximated as $v \approx |w|$ from (3). The equations of motion in the HAT approximation are

$$\frac{du}{dt} = -b|w|u, \quad \frac{dw}{dt} = -b|w|w - g. \quad (19)$$

The solutions are broken into two parts because of |w|. In the ascending part of the trajectory, the solutions are

$$u = \frac{u_0 \cos\varphi}{\cos(\varphi - \omega t)}, \quad w = \sqrt{\frac{g}{b}} \tan(\varphi - \omega \tau), \omega = \sqrt{bg}. \quad (20)$$

$$x = \frac{u_0 \cos\varphi}{\omega} \ln\left[\tan\left(\frac{\pi}{4} - \frac{\varphi}{2} + \frac{\omega\tau}{2}\right) \middle/ \tan\left(\frac{\pi}{4} - \frac{\varphi}{2}\right)\right]$$

$$y = \frac{1}{b} \ln[\cos(\varphi - \omega t)/\cos\varphi], \quad \text{with} \quad \varphi = \tan^{-1}\left(\sqrt{b/g}\, w_0\right). \quad (21)$$

The time it takes to reach the top is $t = \varphi/\omega$. With the values of u, w, x, y in (20,21) at the top as the initial condition for the descending trajectory, the solutions for descent are

$$u = u0 \cos\varphi \frac{\exp(-\omega\tau)}{1 + \exp(-2\omega\tau)}, \quad w = -\sqrt{\frac{g}{b}} \frac{1 - \exp(-2\omega\tau)}{1 + \exp(-2\omega\tau)}, \quad (22)$$

$$x = \frac{u_0 \cos\varphi}{\omega}\left[\frac{\pi}{4} - \tan^{-1}\left(e^{-\omega t}\right) - \ln\tan\left(\frac{\pi}{4} - \varphi/2\right)\right]$$

$$y = \frac{1}{b}\left\{ \ln\left[\frac{2\sqrt{1 + b\omega_0^2/g}}{1 + \exp(-2\omega\tau)}\right] - \omega\tau \right\}. \quad (23)$$

The time τ starts from zero (at the top) in (22, 23).

The trajectories in the HAT approximation are shown in **Figure 1** The best agreement with the full solution is

seen at the highest angle 70°, consistent with the underlying assumptions. We note that the agreement is considerably worse descending than ascending (**Figure 1**, 70° (c)). The reason is that near the top, $w \sim 0$, and the validity of the HAT approximation breaks down, causing the large discrepancy while falling back down. By contrast, the LAT approximation (**Figure 1**, 20° (a)) is valid globally as long as the firing angle is small, giving a much better agreement on both parts of the trajectory.

5. Split-Angle Trajectory (SAT) Approximation

In Sections 3 and 4 we discussed low and high angle trajectories. To be complete, we consider in this section the split angle $\sim \pi/4$, between the LAT and HAT approximations. We assume $u \sim w$. and take the symmetric approach: setting $v \approx \sqrt{2}u$ in the horizontal direction and $v \approx \sqrt{2}|w|$ in the vertical direction. The equations of motion read

$$\frac{du}{dt} = -\sqrt{2}bu^2, \quad \frac{dw}{dt} = -\sqrt{2}b|w|w - g. \quad (24)$$

Note that upon replacing $\sqrt{2}b \to b$ in (24), du/dt is the same as that in (4) of LAT, and dw/dt is the same as that in (19) of HAT. The solutions for u, x will be the same as those in (5,6), and the solutions for w, y will be the same as for w, y in (21,23), so they will not be repeated here.

Similarly, the trajectories can be computed as before (with b replaced by $\sqrt{2}b$, of course). They are also shown in **Figure 1** at the same angles with the same parameters. Here, we see the best agreement with the full solution at 45° as it should. But, unlike the LAT or HAT curves, where after certain point in time (just before reaching the top) the differences keep increasing, the SAT curve crosses the full solution during the course of motion. This is due to the balance of the horizontal and vertical resistance forces.

Because of this balance, the SAT behaviors are interestingly different at low versus high angles. At 20° (**Figure 1(a)**), the SAT curve is "squeezed" horizontally in comparison with the full solution, resulting in a shorter range and a higher height. This is because for low angles where $u > w$, the horizontal resistance is over-estimated in the equations of motion (24). Conversely, at 70° (**Figure 1(c)**), the SAT curve is compressed vertically, causing a lower height but a longer range. The reason is similarly due to the over-estimation of the resistance in the vertical direction. As a result, curve crossing occurs.

6. Conclusions

In summary, we have presented a detailed discussion of projectile motion with quadratic air resistance in three approximations. Our focus was on the low-angle trajec-

tory approximation where we found closed form solutions for the range and the time of flight in terms of the secondary branch of the Lambert W function, W_{-1}. The approximation is simple and accurate for low angle ballistics problems.

Various analytic properties were readily analyzed with these solutions. Together with projectile motion with linear air resistance [1,5], the example studied here serves two educational purposes: i) It is possible to introduce the use of special functions in physics at early undergraduate levels in a familiar, more realistic problem; and ii) It represents a good complimentary case where the physical solution required the secondary branch, W_{-1}, rather than the principal branch W_0 as in the case of linear air resistance.

One interesting and closely-related question remains open, i.e., whether both branches of W might be required simultaneously in a physical solution, say when the air resistance contains both linear and quadratic terms, $-av - bv^2$, under some forms of approximation, presumably.

REFERENCES

[1] R. D. H. Warburton and J. Wang, "Analysis of asymptotic projectile motion with air resistance using the Lambert W function," American Journal of Physics, Vol. 72, pp. 1404–1407, 2004.

[2] S. R. Valluri, D. J. Jeffrey, and R. M. Corless, "Some applications of the Lambert W functions to physics," Canadian Journal of Physics, Vol. 78, pp. 823–830, 2000.

[3] S. R. Cranmer, "New views of the solar wind with the Lambert W function," American Journal of Physics, Vol. 72, pp. 1397–1403, 2004.

[4] D. Razansky, P. D. Einziger, and D. R. Adam, "Optimal dispersion relations for enhanced electromagnetic power deposition in dissipative slabs," Physical Review Letters, Vol. 93, 083902, 2004.

[5] S. M. Stewart, Letters to the Editor, American Journal of

Physics, Vol. 73, pp. 199, 2005. "A little introductory and intermediate physics with the Lambert W function," Proceedings of 16th Australian Institute of Physics, Vol. 005, pp. 194–197, 2005.

[6] E. Lutz, "Analytical results for a Fokker-Planck equation in the small noise limit," American Journal of Physics, Vol. 73, pp. 968–972, 2005.

[7] P. Hövel and E. Schöll, "Control of unstable steady states by time-delayed feedback methods," Physical Review E, Vol. 72, 046203, 2005.

[8] There is a solution presented in terms of the slope angle by A. Tan, C. H. Frick, and O. Castillo, "The fly ball trajectory: An older approach revisited," American Journal of Physics, Vol. 55, pp. 37–40, 1987. But the slope angle is unknown except at the top (zero) of the trajectory, and can be found only numerically or graphically. Therefore, the solution is not in closed form.

[9] G. W. Parker, "Projectile motion with air resistance quadratic in the speed," American Journal of Physics, Vol. 45, pp. 606–610, 1977.

[10] R. M. Corless, G. H. Gonnet, D. E. G. Hare, D. J. Jeffrey, and D. E. Knuth, "On the Lambert W function," Advances in Computational Mathematics, Vol. 5, pp. 329–359, 1996.

[11] H. R. Kemp, "Trajectories of projectile motion in air for small times of flight," American Journal of Physics, Vol. 55, pp. 1099–1102, 1987.

[12] The angle maximizing the range can be derived directly by $\dfrac{dR}{d\vartheta_0} = 0$, from [1], yielding $\left[W(z) + \dfrac{1}{1+\beta} \right] \cos(2\theta_0) = 0$. This implies either $\left[W(z) + \dfrac{1}{1+\beta} \right] = 0$, the trivial unphysical solution, (13); or $\cos(2\theta_0) = 0$, i.e., $\theta_0 = \pi / 4$.

[13] B. Hayes, "Why W?" American Science, Vol. 93, pp. 104–108, 2005.

[14] J. Wang, To be published.

[15] M. Abramowitz and I. A. Stegun, "Handbook of mathematical functions," Dover, New York, pp. 18, 1970.

Appendix

1. The Lambert *W* function

In this appendix, we briefly summarize some relevant elements of the Lambert *W* function. The reader can find an extensive review in [10]. In lieu of the growing interest in this function in the physics community [2–7], we also present several practical formulas for the evaluation of the *W* function.

The Lambert *W* function as defined by (9) is generally complex-valued. For our purpose we are interested in the real-valued *W(x)*, namely the principal branch W_0, and the secondary branch W_{-1}. The two branches are shown in **Figure 3**.

The behaviors of W_0 and W_{-1} for small and large *x* are

$$W_0(x \to 0) = x - x^2 \quad W_{-1}(x \to 0^-) = \ln\left(\frac{x}{\ln x}\right), \quad W_0(x \to \infty) = \ln\left(\frac{x}{\ln x}\right).$$

(A.1)

2. Evaluation of *W*

During the course of our study, we were unable to find in the literature simple and practical algebraic expressions for evaluating *W* over the whole range, and for embedding it in our code. We therefore devised several readily usable approximate formulas given here for this purpose. It should give the interested reader a good starting point in using this function.

W is not (yet) available on a calculator like some elementary functions. It is debatable whether it should be elevated to the status of an elementary function. (See [13] for an enchanting account.) However, one can easily implement it on a programmable calculator with the formulas given here. The accuracy is at least 8 digits, in fact it is usually much better.
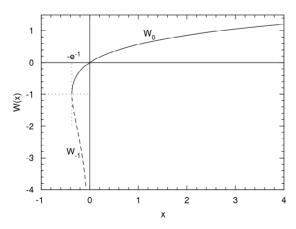

Figure 3. The Lambert *W* function for real argument *x*. The two real branches are the principal branch W_0 (solid line), and the secondary branch W_{-1} (dashed line). The branch point is at $x = -e^{-1}$ where $W = -1$

1) *W* in the Regular Regions

We first give the formulas optimized in the regular regions. Owing to space limitations, we will explain the methods used elsewhere [14]. The general form of the expressions is

$$W_{0,-1}(x) = C + rP(\mathrm{r})$$

(A.2)

where *C* is a constant and $P(\mathrm{r})$ is the Padé approximant defined as

$$P(\mathrm{r}) = \frac{a_0 + a_1 r + a_2 r^2 + a_3 r^3 + a_4 r^4}{1 + b_1 r + b_2 r^2 + b_3 r^3 + b_4 r^4}.$$

(A.3)

The expansion variable, *r*, is related to the independent variable, *x*. We give in **Table 2** the constant *C*, the variable *r*, and the coefficients a_i and b_i. To utilize the table, locate which function and region to use, then evaluate (A.2) with the corresponding *C*, *r*, a_i, and b_i.

2) *W* in the Asymptotic Regions

Both W_0 and W_{-1} have the same form in the asymptotic regions

$$W_{0,-1}(x) = q + (q + q^2)r(1 + a_1 r + a_2 r^2 + a_3 r^3 + a_4 r^4),$$

$$p = \ln\left(\frac{x}{\ln|x|}\right), \quad q = \ln\left(\frac{x}{p}\right), \quad r = \frac{\ln(p/q)}{(1+q)^2}$$

$$a_1 = 1/2, \quad a_2 = (1-2q)/6, \quad a_3 = (1-8q+6q^2)/24,$$

$$a_4 = (1-22q+58q^2-24q^3)/120.$$

(A.4)

This expression (A.4) should be used for W_0 in the region $x \in [2.2, \infty)$ and for W_{-1} in $x \in [-0.12, \infty)$. Note that it is the subtle difference in *p*, namely, $\ln(x/\ln x)$ for W_0 and $\ln[x/\ln(-x)]$ for W_{-1} that automatically selects the correct branch.

3) *W* with a Little Programming

If the reader wishes to calculate *W* with arbitrary precision, one can use Newton's rule [15] which, for a given *x*, is the root, *w*, to $f(w) = w\exp(w) - x = 0$. The root-finding process is as follows: Starting with an initial guess, w_1, the successive iterations, w_n, approach rapidly to the true value as

$$w_{n+1} = \frac{w_n^2 + x\exp(-w_n)}{1 + w_n}, \quad n = 1, 2, 3...$$

(A.5)

It only remains to determine the initial guess, w_1. One way to choose w_1 is

Table 2. The approximate formulas for the evaluation of *W* with (A.2) and (A.3). Spaces are inserted in the coefficients for readability. For optimal precision, all the digits should be used

Function	W_0			W_{-1}
Region	$x \in \left[-e^{-1}, -0.16\right)$	$x \in \left[-0.16, 0.32\right)$	$x \in \left[0.32, 2.2\right)$	$x \in \left[-e^{-1}, -0.12\right)$
Const. *C*	-1	0	0.3906 4638	-1
Variable *r*	$\sqrt{-2\ln(-ex)}$	x	$\ln\left(\sqrt{3}x\right)$	$\sqrt{-2\ln(-ex)}$
a_0	1	1	0.2809 0993	-1
a_1	-0.8040 7820	4.674 4173	0.1116 7016	-0.8178 4020
a_2	0.2802 9706	6.577 4227	0.0 3529 1013	-0.2889 3422
a_3	-0.0 4785 3103	2.730 6731	0.00 5498 1613	-0.0 5003 8980
a_4	0.00 3355 7735	0.1057 7423	0.000 4245 7974	-0.00 3566 1458
b_1	-0.4707 4486	5.674 4173	0.1389 8485	0.4845 0686
b_2	0.0 9560 4321	10.75 1840	0.0 7995 0768	0.0 9965 4140
b_3	-0.00 6612 4586	7.637 5538	0.00 4515 2166	0.00 7066 1014
b_4	$0.7961\ 1402 \times 10^{-5}$	1.539 0142	0.000 6368 7954	$0.5596\ 5023 \times 10^{-5}$

$$w_1 \begin{cases} x & if\ -e^{-1} < x \le 1.5 & W_0 \\ \ln(x) & if\ 1.5 < x < \infty & W_0 \\ \ln(-x) & if\ -e^{-1} < x \le 0 & W_{-1} \end{cases} \quad (A.6)$$

It can be shown [14] that (A.5) with the seed from (A.6) always converges to the correct branch W_0 or W_{-1}. The convergence is fast, usually to machine accuracy in a few iterations.

Summarizing, accurate values for W_0 and W_{-1} over all regions of *x* can be found by using **Table 2** plus (A.4) for fixed precision (8 digits or better), or (A.5) and (A.6) for arbitrary precision.